Superconducting and tetragonal-to-orthorhombic transitions in single crystals of $FeSe_{1-x}Te_x$ ($0 \leq x \leq 0.61$)

Kotaro Terao,[1] Takanari Kashiwagi,[1,2,*] Tomoyuki Shizu,[1] Richard A. Klemm,[3] and Kazuo Kadowaki[1,2,4]

[1]*Graduate School of Pure and Applied Sciences, University of Tsukuba, 1-1-1 Tennodai, Tsukuba, Ibaraki 305-8573, Japan*

[2]*Division of Materials Science, Faculty of Pure and Applied Sciences, University of Tsukuba, 1-1-1 Tennodai, Tsukuba, Ibaraki 305-8573, Japan*

[3]*Department of Physics, University of Central Florida, 4111 Libra Drive, Orlando, Florida 32816-2385, USA*

[4]*Algae-Biomass and Energy System Research and Development Center, University of Tsukuba, 1-1-1 Tennodai, Tsukuba, Ibaraki 305-8572, Japan*

(Received 30 September 2019; revised manuscript received 13 November 2019; published 24 December 2019; corrected 7 April 2020)

Single crystals of $FeSe_{1-x}Te_x$ were grown for $0 \leq x \leq 0.41$ by a flux method and at $x = 0.61$ by chemical vapor transport in order to study the Te substitution effects on the quality of the single crystals and on their superconducting characteristics. From the in-plane resistivity data of the grown crystals, we found that the superconducting transition temperature T_c slightly decreases with increasing the doping level of x up to around $x = 0.2-0.3$, then begins to increase with x at around $x = 0.4$, and reaches a maximum around $x = 0.6$. These experimental facts are contrasted with the results of thin films where T_c increases up to 23 K around $x = 0.2$. We also observed an anomaly in the temperature dependence of the in-plane resistivity due to the tetragonal-to-orthorhombic structural transition T_s, which decreases nearly linearly with increasing x until finally disappearing near $x = 0.5$. These features were not reported in previous studies performed with polycrystalline and thin film samples.

DOI: 10.1103/PhysRevB.100.224516

I. INTRODUCTION

The discovery of superconductivity in the iron-based compound $LaFeAs(O_{1-x}F_x)$ [1] has attracted much attention because it contains Fe atoms as a main component of the electronic state. Among the many classes of present iron-based superconductors (IBSs), FeSe with the PbO structure is structurally the simplest superconductor with transition temperature T_c around 9 K [2]. Unlike other IBSs such as those based upon the $BaFe_2As_2$ system [3], FeSe is superconducting at atmospheric pressure without any chemical doping. However, like many other chalcogenide superconductors, it undergoes a structural transition at T_s around 90 K, without any antiferromagnetic (AFM) ordering [4]. Furthermore, T_c of FeSe was found to be significantly enhanced up to 37 K by pressure, which also suppresses the structural transition [5], and AFM order was found to emerge [6,7]. Therefore, FeSe is an excellent candidate to study the intertwined relationships between superconductivity and structural and magnetic orderings of IBSs. Recently, much higher T_c values were reported in single-layer FeSe films grown on $SrTiO_3$ substrates [8]. These interesting results were argued to be related to the compound's unusual electronic and superconducting properties arising from BCS-BEC crossover effects [9,10].

It is empirically well known that chemical substitution of the constituent atoms can provide important information related to the electronic states of superconductors. Substitution of S into Se of FeSe appears to apply a positive chemical pressure because of the smaller ionic radius of S^{2-} than that of Se^{2-} without changing the number of valence electrons. It was reported that S substitution induces a decrease of T_s down to 80 K and a small increase of T_c up to 10.1 K for $FeSe_{0.91}S_{0.09}$ [11–13]. On the other hand, substitution of Se by Te, another chalcogen, appears to apply a negative chemical pressure because of the larger ionic radius of Te^{2-} than that of Se^{2-}. It is known that more than 50% of Te substitution of Se in FeSe enhances T_c up to 14 K [14–16], and the superconductivity disappears in FeTe at complete substitution. Note that there was a report that both T_s and T_c of FeSe were sensitive not only to chemical substitutions but also to the crystalline disorder [17]. Both values of FeSe were reduced with increasing disorder of samples. As an example, high-quality crystals of FeSe with the residual resistivity ratio (RRR) above 25 showing $T_s \sim 90$ K and $T_c \sim 9$ K were obtained by controlling the crystal growth conditions [17].

Although good-quality single crystals of FeSe are available, the effects of its gradual substitution effects with Te have still been unexplored because of the difficulty in preparing homogeneous single-crystalline samples of $FeSe_{1-x}Te_x$ with $0 < x \leq 0.5$. Furthermore, in this concentration range, the coexistence of two tetragonal phases, which phase separate into domains, even in polycrystalline samples [18–20], was reported. Some experimental results performed in single-crystalline samples supported those results [14].

Imai *et al.* announced that thin films of $FeSe_{1-x}Te_x$ were synthesized throughout the entire concentration range x without any phase separation [21]. Curiously enough, the giant

*kashiwagi@ims.tsukuba.ac.jp

 ©2019 American Physical Society

enhancement of T_c up to 23 K was observed in thin films with x around 0.2, the composition for which the phase separation occurs in bulk samples.

Here, we report on high-quality single-crystal growth of $FeSe_{1-x}Te_x$ ($0 \leq x \leq 0.41$) by a flux method described in Sec. II. Homogeneous crystals with $x = 0.61$ were grown by chemical vapor transport (CVT). The proper growth temperature T conditions depending on the desired Te concentration x were found empirically for the flux method by comparing each sample with samples grown under different conditions. The quality of each grown sample was checked with x-ray diffraction (XRD) and electron probe microanalysis (EPMA) studies. Using these single crystals, we measured the T dependence of the in-plane resistivity. Superconductivity was observed in all samples with x in the range $0 \leq x \leq 0.61$. From these measurements we found that $T_c(x)$ shows a shallow minimum at 5.6 K in the range around $x = 0.2$, then subsequently reaches a maximum value of 14 K around $x = 0.6$, as was known before. Also, the T dependence of the resistivity curves exhibits anomalies at T_s, which appear to represent the tetragonal-to-orthorhombic structural transition. $T_s(x)$ is suppressed nearly linearly in x by Te substitution from 88 K at $x = 0$ to 30 K at $x = 0.41$. This resistivity anomaly at T_s was not reported in previous studies of polycrystalline and even high-quality thin film samples [21], most likely indicating the good quality of our single crystals, which most likely exhibit the proper bulk nature of this system.

II. EXPERIMENT

High-purity powder of Fe (99.999%) and Te (99.999%) and shots of Se (99.9999%) as starting materials were weighed and mixed in the desired nominal composition with an Fe:(Se_x/Te_{1-x}) ratio of 1.1:1, then ground in an agate mortar. The mixture was first sintered in vacuum at 450 °C in a box furnace for 24 h. Single crystals of $FeSe_{1-x}Te_x$ ($0 \leq x \leq 0.41$) were then grown by the flux method in a two-zone furnace using a flux mixture of $AlCl_3$ and KCl [22], as described in detail in the following.

The presintered mixture of starting materials, typically 0.3 g in mass, was loaded into a quartz tube with a mixture of $AlCl_3$ and KCl, which typically had a combined mass of 3 g. After loading, the tube was evacuated to less than 2 Pa and sealed off. Then, the quartz tube was covered by a stainless-steel tube in order to protect it from a possible explosion when the temperature exceeds 600 °C. All mixing and weighing procedures were performed in an Ar-filled glove box in order to prevent possible oxidation and hydration. The quartz tube was then placed in a horizontal two-zone tube furnace, as schematically depicted in Fig. 1(a). The temperature of the hotter part T_{hot} was kept at 500 °C–650 °C, and that of the colder part T_{cold} was kept at 300 °C–500 °C. The details of the two-zone furnace temperature setting conditions for the growth of each desired crystal composition are shown in Table I. After 20–30 days, the quartz tube was removed from the furnace and quenched into cold water. The residual flux was removed by dissolving it in distilled water in order to isolate the desired single crystals. An optical photograph of the resulting platelike single crystals with shiny surfaces is shown in Fig. 1(b).

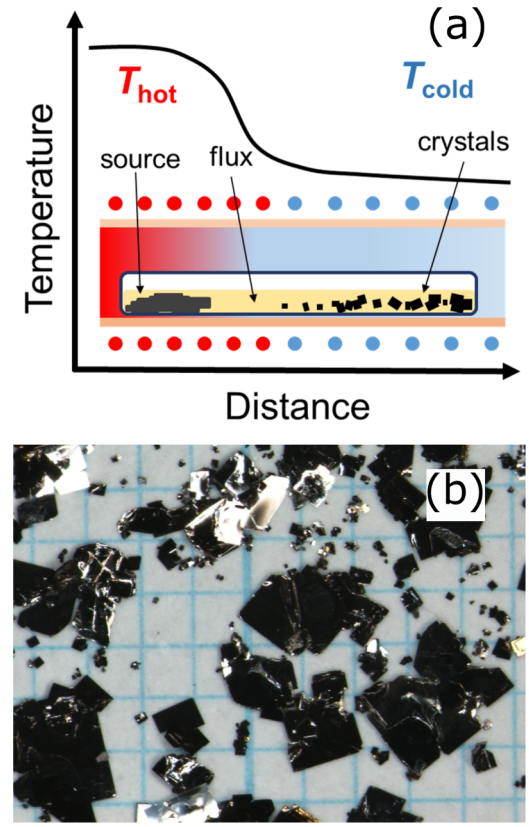

FIG. 1. (a) Schematic image of the temperature distribution in the horizontal tube furnace for single-crystal growth of $FeSe_{1-x}Te_x$ by the flux method. The crystallization takes place at the cold end of the furnace. Temperature pairs of T_{hot} and T_{cold} are selected depending on x. (b) Photograph of as-grown single crystals of $FeSe_{1-x}Te_x$ nominally with $x = 0.3$ after removing the flux.

We have also tried the CVT method to grow single crystals with $AlCl_3$ and KCl [17,23,24] or I_2 as transport agents. However, those CVT attempts were not successful in obtaining $FeSe_{1-x}Te_x$ single crystals with x satisfying $0 < x \leq 0.5$. Therefore, presently, the flux method using $AlCl_3$ + KCl as the flux agents is the most promising method to grow homogeneous single crystals with x below 0.5. However, single crystals of $FeSe_{0.39}Te_{0.61}$ were grown by the CVT method with iodine as the transport agent for comparison.

The structures of the obtained single crystals were characterized by an x-ray diffractometer (PANalytical). Their chemical compositions were quantitatively estimated with an electron probe microanalyzer (JEOL). The composition x of

TABLE I. Crystal growth conditions of $FeSe_{1-x}Te_x$. The Te concentration x is estimated by EPMA measurements.

Nominal (%)	T_{hot} (°C)	T_{cold} (°C)	Growth time (days)	x (%)
0	400	300	30	0
0.14	500	300	20	0.04, 0.08, 0.19
0.33	600	380	22	0.3*
0.33	610	520	22	0.30, 0.41

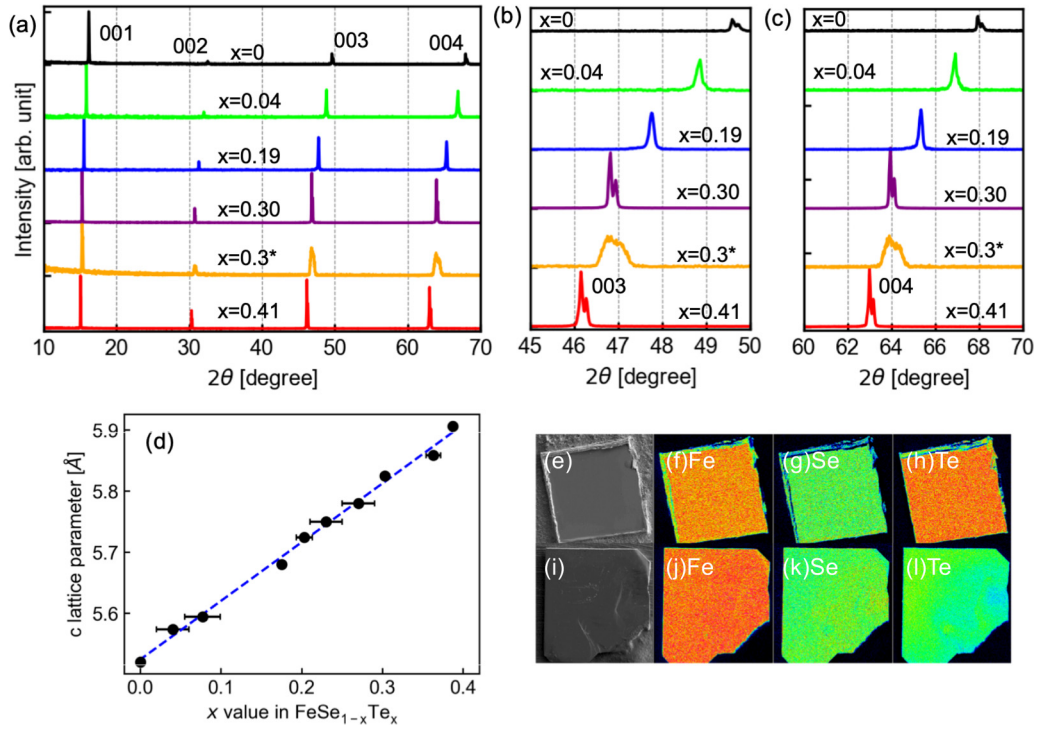

FIG. 2. (a) X-ray diffraction patterns of $FeSe_{1-x}Te_x$ ($x = 0$, 0.04, 0.19, 0.30, 0.3*, 0.41) single crystals; (b) and (c) the magnified plots at around the (003) and (004) reflections. Except for the bottom $x = 0.41$ data, the intensities are offset for clarity. (d) Substitution x dependence of the c-axis lattice parameters of $FeSe_{1-x}Te_x$ ($x = 0$–0.41). The dashed line is a linear fit to the data. (e) SEM image and elemental mappings of (f) Fe, (g) Se, and (h) Te measured on the sample with $x = 0.30$. (i) SEM image and elemental mappings of (j) Fe, (k) Se, and (l) Te measured on the sample with $x = 0.3^*$, which contains an inhomogeneous distribution of Se and Te, as can be seen clearly in (k) and (l).

Te was estimated by averaging over the EPMA data obtained at several different positions in each single crystal. The in-plane resistivity was measured by the standard four-probe method using an AC resistance bridge. Electrical leads were attached to the gold pads placed on the cleaved surface of the samples by evaporation with silver paste.

III. RESULTS AND DISCUSSION

Single crystals of $FeSe_{1-x}Te_x$ ($0 \leq x \leq 0.41$) were grown by the $AlCl_3$ + KCl flux method. The crystal growth is schematically shown in Fig. 1(a). The proper temperature conditions, depending on the desired composition x of Te, were examined in detail, and the best conditions are summarized in Table I. It became clear that the estimated values of x by EPMA measurements depend on the starting nominal composition and the temperature gradient determined by T_{hot} and T_{cold}. We note also that the thickness of the obtained crystals appears to increase with decreasing x values according to the temperature conditions shown in Table I. In Fig. 1(b), as-grown single crystals of $FeSe_{1-x}Te_x$ (nominal $x = 0.3$) after removing the flux are displayed. Square-plate single crystals with lateral dimensions up to $2 \times 2\,mm^2$ were obtained.

We note that for the particular case of the nominal composition x of 0.14, we obtained several crystals with distinctly different final x values within a single sample batch. This result strongly suggests that the control of x is very sensitive to the growth temperatures of the flux solution, which can depend upon the particular position in the quartz tube. We also found that in order to increase the substitution level of x, we need a higher-temperature set of both T_{hot} and T_{cold}. Typically, in the low substitution level ($x = 0$–0.2), the set of $T_{cold} = 300\,^\circ C$ and $T_{hot} = 500\,^\circ C$ was a successful condition, whereas the temperature set of $T_{cold} = 520\,^\circ C$ and $T_{hot} = 610\,^\circ C$ gave a good result in the intermediate-substitution level ($x = 0.3$–0.4). This feature is probably related to the fact that PbO-type single-crystal formation of FeSe occurs at a lower optimum temperature than does that of FeTe [25,26].

Typical x-ray diffraction intensity data from single crystals of $FeSe_{1-x}Te_x$ with (top to bottom) $x = 0$, 0.04, 0.19, 0.30, 0.3*, and 0.41 are shown in Fig. 2(a). We observed sharp diffraction peaks that can be attributed to the (00ℓ) reflection lines. Figures 2(b) and 2(c) show magnifications of Fig. 2(a) around the (003) and (004) reflections corresponding to around $2\theta = 45^\circ$ and 65°, respectively. These results indicate good crystallinity and also suggest a uniform random substitution of Se and Te ions, except for the case of $x = 0.3^*$. In Figs. 2(k) and 2(l), the inhomogeneous mixture of Se and Te is seen for $x = 0.3^*$. No trace of a second tetragonal phase formation was found in this XRD study.

It is clear that the peaks shift to lower scattering angles 2θ with increasing x. In addition, the sharp splittings of the (00ℓ) peaks due to the Cu $K\alpha_1$ and Cu $K\alpha_2$ radiation were clearly observed for the samples with $x = 0$, 0.30, and 0.41, suggesting highly homogeneous distributions of x in the latter two of those crystals. On the other hand, the peaks of the other samples with ($0 < x < 0.30$) are not clearly split but are broadened. This broadening may possibly be due to an

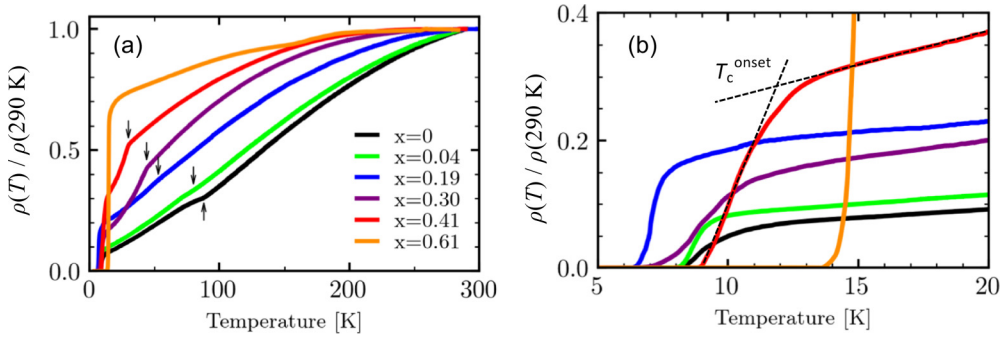

FIG. 3. (a)Temperature dependence of in-plane resistivity of $FeSe_{1-x}Te_x$ single crystals for $x = 0$, 0.04, 0.19, 0.30, 0.41, 0.61, normalized by its respective value at 290 K. Black arrows indicate the anomalies due to structural transitions, whose T_s values are determined accurately by examining the derivative curves, dR/dT. (b) Magnified plots of the normalized resistivity curves shown in (a) for 5 K $\leq T \leq$ 20 K. T_c^{onset} is defined as the temperature of the crossing point of the linear fit to the resistivity curve in the normal state and the slope curve just above the superconducting transition. The superconducting transition temperature T_c is defined to be the highest temperature at which the resistivity is zero.

inhomogeneous distribution of Te and Se within the crystals for those compositions, effectively forming clusters of higher and lower Te concentration regions in a single crystal. It should be noted that those samples with broad peaks are contrasted with the results of a clear separation of two tetragonal phases in the crystal observed previously [18–20].

The substituted concentration dependence of the c-axis lattice parameters is shown in Fig. 2(d). The c-axis length was found to increase almost linearly with increasing x, consistent with the substitution of Se sites by Te in this concentration range. This result suggests that the substitution of the Se site by a larger atomic radius ion of Te expands the lattice constant of $FeSe_{1-x}Te_x$ single crystals in a manner proportional to the Te concentration.

There are distinct differences between the samples with $x = 0.30$ and $x = 0.3^*$. The sample with $x = 0.30$ was grown under a relatively small temperature gradient of $\Delta T = T_{hot} - T_{cold} \sim 100\,^\circ$C, whereas the sample of $x = 0.3^*$ was grown under the larger temperature gradient $\Delta T \sim 200\,^\circ$C. As displayed in Figs. 2(b) and 2(c), the sample with $x = 0.3^*$ shows significantly wider XRD peak widths than that with $x = 0.30$. We interpret this broadening effect as arising from an inhomogeneous distribution of Se and Te ions in the sample. This feature is clearly detected in the EPMA compositional mapping shown in Figs. 2(e)–2(l). In the case of $x = 0.30$, the homogeneous distributions of Fe, Se, and Te ions are clearly seen. In sharp contrast to this, the EPMA mapping data of $x = 0.3^*$ shows inhomogeneities in the distributions of Se and Te ions. Evidence of such an inhomogeneous distribution of Se and Te ions was also reported in $FeSe_{0.39}Te_{0.61}$[27]. By comparing the XRD and the EPMA results for $x = 0.3^*$ and $x = 0.30$, our results suggest that maintaining a proper temperature gradient is very important to synthesize homogeneous single crystals of $FeSe_{1-x}Te_x$.

In the case of vapor-grown FeSe crystals reported by Böhmer *et al.* [17], the most uniform quality crystals were obtained with the nominal Fe:Se ratio of 1.1:1 and a small, well-controlled temperature gradient of 350 °C–390 °C. In addition, not only the shapes but also the quality of crystals of the FeSe crystals as estimated by the relation of their RRR values to disorder are very sensitive to the temperature gradient conditions of the crystal growth. According to our results and to those of the above study, the temperature gradient conditions of the crystal growth are essential not only for the quality of the crystals but also for the Te substitution level of FeSe.

We have studied the effects of Te substitution of FeSe on the in-plane resistivity and upon T_c. Figure 3 shows the temperature dependence of the in-plane resistivity of $FeSe_{1-x}Te_x$ ($x = 0$–0.41), normalized by its respective value at 290 K. For comparison, the similarly normalized resistivity of a single crystal of $FeSe_{0.39}Te_{0.61}$ grown by CVT is also displayed.

As seen in Fig. 3(a), the normalized resistivities increase systematically with x in the substitution range from $x = 0$ to $x = 0.61$ for $T_{c,max} \leq T \leq 290$ K, where $T_{c,max}$ is the maximum T_c of the samples shown. In addition, each normalized resistivity curve shows metallic behavior, exhibiting $d\rho/dT > 0$ over its entire T range, $T_c \leq T \leq 290$ K. This latter feature is in sharp contrast to the resistivity data obtained from samples including excess iron atoms, each of which shows a semiconductorlike upturn in $\rho(T)/\rho(290\ K)$ as T decreases from 290 K. Note that by annealing such samples appropriately with oxygen, this upturn can be suppressed due to the reduction of the excess iron atoms [28]. The clear differences between the present data and the previous ones indicate that the present single crystals of $FeSe_{1-x}Te_x$ most likely contain considerably fewer unoxidized Fe atoms.

The superconducting transition temperature T_c is defined to be the highest temperature at which the resistivity is zero. All samples studied show zero resistivity at and below T_c, as depicted in Fig. 3(b). Note that T_c^{onset} was defined by the intersection of the two dashed extrapolation lines shown in Fig. 3(b). For example, T_c^{onset} of the sample with $x = 0.30$ is determined to be 11.2 K, although its resistivity already starts to drop significantly at rather higher temperatures around 14 K.

We observed anomalies in the temperature dependence of the resistivity for $0 \leq x \leq 0.41$, which are indicated by the black arrows in Fig. 3 in all curves except that for $x = 0.61$. These anomalies are attributed to the tetragonal-to-orthorhombic structural transition. That structural transition temperature T_s is determined more accurately from the

TABLE II. Superconducting transition temperature T_c^{onset}, T_c, structural transition temperature T_s, resistivity ρ at 290 K, ρ_{res}, and RRR for $FeSe_{1-x}Te_x$ single crystals ($x = 0$–0.61).

x (%)	T_c^{onset} (K)	T_c (K)	T_s (K)	ρ(290 K) (mΩ cm)	ρ_{res} (mΩ cm)	RRR
0	10.0	8.3	~88	0.48	2.73×10^{-2}	17.6
0.04	9.3	8.1	~80	0.60	4.92×10^{-2}	12.2
0.19	7.5	5.6	~53	0.91	0.16	5.7
0.30	10.2	7.2	~44	0.56	7.67×10^{-2}	7.3
0.41	11.2	9.1	~30	0.59	0.19	3.1
0.61	15.0	14.0		0.41	0.27	1.5

respective dR/dT curve for each x. As shown in Fig. 3(a), T_s decreases systematically with increasing x. This feature was not reported in thin films [21] and in the phase-separated polycrystalline samples of $FeSe_{1-x}Te_x$ [18–20].

The above-mentioned T_c^{onset}, T_c, T_s, ρ(290 K), $\rho_{res} \equiv \rho(T_c^{onset})$, and RRR $\equiv \rho(290K)/\rho(T_c^{onset})$ values are summarized in Table II. Except at $x = 0.19$, the RRR decreases monotonically with increasing x. The low RRR value (~1.5) of the sample with $x = 0.60$ is comparable to previously reported data [14–16,28]; however, this concentration exhibits an optimal value of T_c. It is also noted that the higher ρ(290 K) and ρ_{res} values and hence the lower RRR value of the sample with $x = 0.19$ may be due to its poorer crystallinity than those of the other samples. This plausible explanation is consistent with the XRD data shown in Fig. 2, in which the two Cu $K\alpha$ peaks were not resolvable for that sample.

According to the above experimental data, we made a superconducting phase diagram of the $FeSe_{1-x}Te_x$ system, as shown in Fig. 4. In $0 \leq x \leq 0.61$, T_s and T_c were obtained from our resistivity measurement, while in $0.6 \leq x \leq 1$, T_c and the AFM transition temperature T_N, determined by magnetic susceptibility measurements, were taken from the literature [16]. The Te substitution level x was determined by the EPMA method as described above.

Interestingly, T_c exhibits a broad minimum around $x \sim 0.2$ and a broad maximum in the range $x = 0.5$–0.7. In addition, T_s of $FeSe_{1-x}Te_x$ decreases monotonically, almost linearly within the error, with increasing x, indicating suppression of the structural transition by the Te substitution. Since T_c attains its maximum value after T_s is fully suppressed, these two transitions appear to compete with one another. A broad minimum of T_c around $x \sim 0.2$ may be attributed to the effect of sample disorder, as discussed by Böhmer *et al.* [17] According to their study, the reduction of both T_c and T_s correlates with decreasing RRR values, which are related to the disorder of the samples. This feature is probably reflected in the small x region.

Similar features between T_c and T_s are also reported in the pressure vs T_c phase diagram of FeSe [7] and the S substitution effects [12]. In the case of FeSe under pressure, at first T_c is enhanced to ~13 K with pressure up to around 8 kbar; then T_c shows a broad minimum at around 12 kbar, after which T_c increases up to around 20 K with increasing pressure up to 25 kbar. T_s of FeSe becomes small almost linearly with increasing pressure up to 20 kbar. The maximum T_c of FeSe under pressure appears to occur at the pressure at which T_s is first fully suppressed.

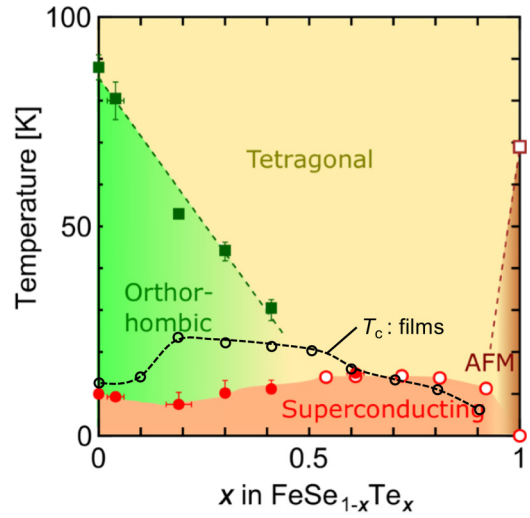

FIG. 4. Temperature phase diagram of $FeSe_{1-x}Te_x$ single crystals as a function of x. The red solid circles and the green solid squares represents T_c and T_s, respectively. Those values are deduced from our resistivity measurements. The green dashed line is a least-squares fit to the $T_s(x)$ data. On the other hand, red open circles for T_c and a brown open square for T_N are values taken from a previous report [16]. Vertical bars of T_c denote the onset of the transition temperature, and horizontal bars denote the standard deviation of x estimated by EPMA. T_c values for thin films [21] are plotted by the open black circles with a dashed curve that is an eye guide.

Thus, for FeSe, both T_c and T_s are modified by a positive pressure. Our Te substitution studies correspond to a negative pressure due to the expansion of the c-axis lattice constant, consistent with the ionic radius expansion and as shown in Fig. 2(b). Thus, the observed behaviors show similarities between the two systems. These results strongly suggest that the reduction of the orthorhombic distortion plays a key role in the enhancement of T_c.

In order to study further this phase diagram, we compared our data obtained from bulk single crystals with those obtained from thin films. We first provide a brief explanation of the phase diagram. T_c of the FeSe thin film at $x = 0$ is about 12 K, which is slightly higher than that of our bulk sample. T_c is suddenly enhanced around $x = 0.1$ to 0.2; then a maximum T_c of 23 K is observed at $x = 0.2$. Basically, T_c decreases with increasing x up to $x = 0.9$. These features are also displayed in Fig. 4. According to the explanation of the authors who studied the thin films, decreasing T_c above $x = 0.2$ can be understood from the bond angle between the chalcogen and Fe and the anion height above the iron plane.

Next, we discuss the phase diagram as it relates to the c-axis lattice constant. Our data for the x concentration dependence of the c-axis lattice constants are very similar to those for the thin films. The lattice constant of the c axis in both systems shows almost a linear increase with increasing Te composition x. However, at $x = 0.2$, T_c of the thin film has its maximum value of 23 K, whereas the bulk crystal shows its minimum T_c of 5.6 K. This difference cannot be understood from the modification of the c-axis lattice constant

alone. In addition, as mentioned above, the samples with x values above $x = 0.2$ have decreasing T_c in thin films, whereas T_c of the bulk crystals increase with x up to $x = 0.6$. This opposite behavior is difficult to understand and cannot be explained simply from the change in the c-axis lattice constants. These results strongly suggest that the modification of the c axis seems to induce different effects in the above two systems. This difference might be related to the orthorhombic distortion of the crystals discussed below.

Finally, we discuss further the tetragonal-to-orthorhombic structural transition. When our single-crystal resistivity data are compared with those obtained from thin films, the T_c values of which are strongly enhanced for $(0.2 \leq x \leq 0.4)$ and even exceed 20 K, the phase diagrams appear very different, as mentioned above. In addition to the difference in $T_c(x)$ between the two systems, a remarkable difference between them occurs in the tetragonal-to-orthorhombic structural transition at T_s, which is clearly seen in the temperature dependence of the resistivity of bulk single crystals. The enhancement of T_c of thin films in the range $(0.2 \leq x \leq 0.4)$ may be due to the absence of the structural transition T_s in thin films due perhaps to the strain (or effective pressure) from the substrate. This result strongly suggests that the orthorhombic distortion from the tetragonal structure suppresses the superconductivity in the $FeSe_{1-x}Te_x$ system. However, further studies such as Shubnikov–de Haas oscillations, specific heat, and magnetic properties are certainly required in order to clarify more details of how this orthorhombic distortion modifies the electronic structure of $FeSe_{1-x}Te_x$. We consider these topics to be of primary interest for future studies.

IV. SUMMARY

We reported on the growth of high-quality single crystals of $FeSe_{1-x}Te_x$ by the $AlCl_3$ + KCl flux method. We showed that sufficiently improved single crystals can be grown by empirically finding the proper dual-temperature conditions, each of which depends upon the Te concentration x. For low substitution levels, $x = 0$–0.2, $T_{cold} = 300\,^{\circ}C$ and $T_{hot} = 500\,^{\circ}C$ were the most successful pair of conditions, while the set of $T_{cold} = 520\,^{\circ}C$ and $T_{hot} = 610\,^{\circ}C$ was found to be adequate in the middle substitution level ($x = 0.3$–0.4). The XRD, the EPMA, and resistivity measurement data clearly proved the substitution of Te for Se into the grown crystals. The temperature dependence of the resistivity exhibits superconductivity in all samples. It was found that $T_c(x)$ shows a minimum in the range around $x = 0.2$ and then, as x is increased, reaches a maximum around $x = 0.6$. This result is in sharp contrast to results for thin films. The resistivity curves also exhibit anomalies at T_s corresponding to the tetragonal-to-orthorhombic structural transition, which are suppressed by Te substitution from 88 K in $x = 0$ to 30 K in $x = 0.41$. This anomaly corresponding to a structural transition was not reported in the previous studies performed on polycrystalline and thin-film samples, further indicating the bulk nature of the present crystals. From these results, an interesting conclusion can be put forward in which the superconducting transition temperature T_c is suppressed very sensitively by the crystallographic tetragonal to orthorhombic phase transition. However, T_c is very insensitive to other substitution effects, such as the c-axis lattice parameter, and disorder effects of Te and Se, leading to the residual resistance. This competition between the structural and superconducting transitions is very similar to the competition between the spin- and charge-density waves and the superconducting transitions in the organic and transition-metal dichalcogenide layered superconductors, respectively, and to the competition between the so-called pseudogap and the superconducting state in the cuprates [29,30]. These properties should be carefully taken into account in considering the mechanism of superconductivity in the $FeSe_{1-x}Te_x$ system.

ACKNOWLEDGMENTS

This study was supported by JSPS KAKENHI Grant Number JP15H01996. T.K. was supported by JSPS KAKENHI Grant Number JP17K05018 and TIA collaborative research program.

[1] Y. Kamihara, T. Watanabe, M. Hirano, and H. Hosono, J. Am. Chem. Soc. **130**, 3296 (2008).

[2] F.-C. Hsu, J.-Y. Luo, K.-W. Yeh, T.-K. Chen, T.-W. Huang, P. M. Wu, Y.-C. Lee, Y.-L. Huang, Y.-Y. Chu, D.-C. Yan, and M.-K. Wu, Proc. Natl. Acad. Sci. USA **105**, 14262 (2008).

[3] M. Rotter, M. Tegel, and D. Johrendt, Phys. Rev. Lett. **101**, 107006 (2008).

[4] T. M. McQueen, A. J. Williams, P. W. Stephens, J. Tao, Y. Zhu, V. Ksenofontov, F. Casper, C. Felser, and R. J. Cava, Phys. Rev. Lett. **103**, 057002 (2009).

[5] J. Sun, K. Matsuura, G. Z. Ye, Y. Mizukami, M. Shimozawa, K. Matsubayashi, M. Yamashita, T. Watashige, S. Kasahara, Y. Matsuda, J. Q. Yan, B. C. Sales, Y. Uwatoko, J. G. Cheng, and T. Shibauchi, Nat. Commun. **7**, 12146 (2016).

[6] S. Medvedev, T. M. McQueen, I. A. Troyan, T. Palasyuk, M. I. Eremets, R. J. Cava, S. Naghavi, F. Casper, V. Ksenofontov, G. Wortmann *et al.*, Nat. Mater. **8**, 630 (2009).

[7] T. Terashima, N. Kikugawa, S. Kasahara, T. Watashige, T. Shibauchi, Y. Matsuda, T. Wolf, A. E. Böhmer, F. Hardy, C. Meingast, H. v Löhneysen, and S. Uji, J. Phys. Soc. Jpn. **84**, 063701 (2015).

[8] J. Ge, Z. Liu, C. Liu, C. Gao, D. Qian, Q. Xue, Y. Liu, and J. Jia, Nat. Mater. **14**, 285 (2015).

[9] S. Kasahara, T. Watashige, T. Hanaguri, Y. Kohsaka, T. Yamashita, Y. Shimoyama, Y. Mizukami, R. Endo, H. Ikeda, K. Aoyama *et al.*, Proc. Natl. Acad. Sci. USA **111**, 16309 (2014).

[10] S. Kasahara, T. Yamashita, A. Shi, R. Kobayashi, Y. Shimoyama, T. Watashige, K. Ishida, T. Terashima, T. Wolf, F. Hardy, C. Meingast, H. v. Löhneysen, A. Levchenko, T. Shibauchi, and Y. Matsuda, Nat. Commun. **7**, 12843 (2016).

[11] M. Abdel-Hafiez, Y. Y. Zhang, Z. Y. Cao, C. G. Duan, G. Karapetrov, V. M. Pudalov, V. A. Vlasenko, A. V. Sadakov, D. A. Knyazev, T. A. Romanova, D. A. Chareev, O. S. Volkova, A. N. Vasiliev, and X. J. Chen, Phys. Rev. B **91**, 165109 (2015).

[12] S. A. Moore, J. L. Curtis, C. DiGiorgio, E. Lechner, M. Abdel-Hafiez, O. S. Volkova, A. N. Vasiliev, D. A. Chareev, G. Karapetrov, and M. Iavarone, Phys. Rev. B **92**, 235113 (2015).

[13] M. D. Watson, T. K. Kim, A. A. Haghighirad, S. F. Blake, N. R. Davies, M. Hoesch, T. Wolf, and A. I. Coldea, Phys. Rev. B **92**, 121108(R) (2015).

[14] B. C. Sales, A. S. Sefat, M. A. McGuire, R. Y. Jin, D. Mandrus, and Y. Mozharivskyj, Phys. Rev. B **79**, 094521 (2009).

[15] C. Dong, H. Wang, Z. Li, J. Chen, H. Q. Yuan, and M. Fang, Phys. Rev. B **84**, 224506 (2011).

[16] T. Noji, T. Suzuki, H. Abe, T. Adachi, M. Kato, and Y. Koike, J. Phys. Soc. Jpn. **79**, 084711 (2010).

[17] A. E. Böhmer, V. Taufour, W. E. Straszheim, T. Wolf, and P. C. Canfield, Phys. Rev. B **94**, 024526 (2016).

[18] M. H. Fang, H. M. Pham, B. Qian, T. J. Liu, E. K. Vehstedt, Y. Liu, L. Spinu, and Z. Q. Mao, Phys. Rev. B **78**, 224503 (2008).

[19] Y. Mizuguchi, F. Tomioka, S. Tsuda, T. Yamaguchi, and Y. Takano, J. Phys. Soc. Jpn. **78**, 074712 (2009).

[20] K.-W. Yeh, T.-W. Huang, Y.-l. Huang, T.-K. Chen, F.-C. Hsu, P. M. Wu, Y.-C. Lee, Y.-Y. Chu, C.-L. Chen, J.-Y. Luo *et al.*, Europhys. Lett. **84**, 37002 (2008).

[21] Y. Imai, Y. Sawada, F. Nabeshima, and A. Maeda, Proc. Natl. Acad. Sci. USA **112**, 1937 (2015).

[22] D. Chareev, E. Osadchii, T. Kuzmicheva, J.-Y. Lin, S. Kuzmichev, O. Volkova, and A. Vasiliev, CrystEngComm **15**, 1989 (2013).

[23] A. E. Böhmer, F. Hardy, F. Eilers, D. Ernst, P. Adelmann, P. Schweiss, T. Wolf, and C. Meingast, Phys. Rev. B **87**, 180505(R) (2013).

[24] S. Karlsson, P. Strobel, A. Sulpice, C. Marcenat, M. Legendre, F. Gay, S. Pairis, O. Leynaud, and P. Toulemonde, Supercond. Sci. Technol. **28**, 105009 (2015).

[25] T. M. McQueen, Q. Huang, V. Ksenofontov, C. Felser, Q. Xu, H. Zandbergen, Y. S. Hor, J. Allred, A. J. Williams, D. Qu *et al.*, Phys. Rev. B **79**, 014522 (2009).

[26] H. Okamoto and L. E. Tanner, in *Binary Alloy Phase Diagrams*, edited by T. B. Massalski (ASM International, Cleveland, OH, 1990), Vol. 2, p. 1781.

[27] T. Taen, Y. Tsuchiya, Y. Nakajima, and T. Tamegai, Phys. Rev. B **80**, 092502 (2009).

[28] Y. Sun, T. Taen, T. Yamada, S. Pyon, T. Nishizaki, Z. Shi, and T. Tamegai, Phys. Rev. B **89**, 144512 (2014).

[29] R. A. Klemm, Phys. C (Amsterdam, Neth.) **341–348**, 839 (2000).

[30] R. A. Klemm, Phys. C (Amsterdam, Neth.) **514**, 86 (2015).

Correction: Axis labeling in Fig. 3 was rendered incorrectly during the conversion process and has been fixed.